Monthly Notices
of the
ROYAL ASTRONOMICAL SOCIETY

MNRAS **447,** 3311–3321 (2015) doi:10.1093/mnras/stu2724

Misalignment between cold gas and stellar components in early-type galaxies

O. Ivy Wong,[1⋆] K. Schawinski,[2] G. I. G. Józsa,[3,4,5] C. M. Urry,[6,7] C. J. Lintott,[8] B. D. Simmons,[8] S. Kaviraj[8,9] and K. L. Masters[10,11]

[1]*International Centre for Radio Astronomy Research, The University of Western Australia M468, 35 Stirling Highway, Crawley, WA 6009, Australia*
[2]*Institute for Astronomy, ETH Zürich, Wolfgang-Pauli-Strasse 27, CH-8093 Zürich, Switzerland*
[3]*SKA South Africa, Radio Astronomy Research Group, 3rd Floor, The Park, Park Road, Pinelands 7405, South Africa*
[4]*Rhodes Centre for Radio Astronomy Techniques and Technologies, Department of Physics and Electronics, Rhodes University, PO Box 94, Grahamstown 6140, South Africa*
[5]*Argelander Institut für Astronomie (AIfA), University of Bonn, Auf dem Hügel 71, D-53121 Bonn, Germany*
[6]*Yale Center for Astronomy and Astrophysics and Department of Physics, Yale University, PO Box 208120, New Haven, CT 06520-8120, USA*
[7]*Department of Astronomy, Yale University, PO Box 208101, New Haven, CT 06520-8101, USA*
[8]*Oxford Astrophysics, Denys Wilkinson Building, Keble Road, Oxford OX1 3RH, UK*
[9]*Centre for Astrophysics Research, University of Hertfordshire, College Lane, Hatfield, Herts AL10 9AB, UK*
[10]*Institute of Cosmology and Gravitation, University of Portsmouth, Dennis Sciama Building, Portsmouth PO1 3FX, UK*
[11]*South East Physics Network (SEPNet), www.sepnet.ac.uk*

Accepted 2014 December 17. Received 2014 December 17; in original form 2014 September 15

ABSTRACT

Recent work suggests blue ellipticals form in mergers and migrate quickly from the blue cloud of star-forming galaxies to the red sequence of passively evolving galaxies, perhaps as a result of black hole feedback. Such rapid reddening of stellar populations implies that large gas reservoirs in the pre-merger star-forming pair must be depleted on short time-scales. Here we present pilot observations of atomic hydrogen gas in four blue early-type galaxies that reveal increasing spatial offsets between the gas reservoirs and the stellar components of the galaxies, with advancing post-starburst age. Emission line spectra show associated nuclear activity in two of the merged galaxies, and in one case radio lobes aligned with the displaced gas reservoir. These early results suggest that a kinetic process (possibly feedback from black hole activity) is driving the quick truncation of star formation in these systems, rather than a simple exhaustion of gas supply.

Key words: galaxies: elliptical and lenticular, cD – galaxies: evolution – galaxies: formation.

1 INTRODUCTION

Star-forming galaxies show a correlation between stellar mass and star formation rate whose normalization varies with redshift, but whose scatter remains tight out to high redshift (Noeske et al. 2007; Peng et al. 2010; Elbaz et al. 2011). This correlation can be explained as a balance between gas inflows from cosmological scales and outflows driven by supernovae (Bouché et al. 2010; Lilly et al. 2013). Quenching of star formation causes galaxies to depart from this steady state along pathways that depend on the evolution of the gas supply and reservoir (Schawinski et al. 2014): if the cosmological gas supply to a galaxy is shut off, it will slowly exhaust its gas reservoir by forming stars at a declining rate. If instead the gas reservoir fuelling star formation is destroyed effectively instantaneously, then star formation will cease and the galaxy will redden rapidly within 1 Gyr, as is observed in early-type galaxies (ETGs; Kaviraj et al. 2011; Wong et al. 2012; Schawinski et al. 2014). Interestingly, this time-scale of 1 Gyr is consistent with that proposed for the transition of a merger-driven ultraluminous infrared galaxy (ULIRG) to an ETG (Emonts et al. 2006). Also, it has been known for a while that ULIRGs have a high merger fraction (Sanders et al. 1988).

In addition, negative feedback from a galaxy's central active galactic nuclei (AGN) has often been invoked in galaxy formation models to slow down the star formation history of simulated galaxies (e.g. Croton et al. 2006). However, observational evidence for such feedback is currently only available for a few individual galaxies (Kharb et al. 2006; Croston et al. 2008; Alatalo et al. 2011; Hota et al. 2011; Nyland et al. 2013; Harrison et al. 2014). With the advent of very large surveys, much progress has been made towards understanding of the co-evolution between galaxies and their central

⋆ E-mail: ivy.wong@uwa.edu.au

AGN, in particular the connection between classical bulges and central supermassive black holes (Kormendy & Ho 2013; Heckman & Best 2014).

Blue ETGs do not fit the canonical bimodal scheme of red ellipticals versus blue spirals and are unlikely to be the descendants of blue spirals (Tojeiro et al. 2013). Rather, the blue ETGs appear to be transition-type galaxies and are probable predecessors of local post-starburst galaxies (Schawinski et al. 2009b; Wong et al. 2012). Previous CO observations of blue ETGs show that the molecular gas reservoirs are being rapidly destroyed during the composite star formation and AGN phase (Schawinski et al. 2009a). Local post-starburst galaxies are defined to be galaxies which have recently ceased forming stars. These galaxies typically show little Hα or [O II] emission (indicative of current star formation), but have strong absorption line signatures indicative of a young stellar population. In addition, local post-starbursts consist mostly of galaxies which have similar early-type structural properties to red sequence galaxies of comparable masses (Wong et al. 2012).

Earlier attempts to map the H I content of post-starburst galaxies only found H I in one of five targets which consisted of an interacting pair of galaxies (Chang et al. 2001). All subsequent campaigns to detect H I in post-starbursts have been optimized towards detecting diffused low surface brightness gas, while compromising on the angular resolution required to map the location of the gas (e.g. Zwaan et al. 2013).

To determine the physical process responsible for shutting down star formation, we posit that post-starburst galaxies are too evolved and that *the smoking gun for quenching is more likely to be found in its predecessor population, namely, the blue ETGs.*

Using the Westerbork Syntheses Radio Telescope (WSRT), we study the H I content of a pilot sample of four blue ETGs – the progenitors to post-starburst galaxies – because (1) these galaxies are still currently star forming and therefore there should be gas where there are stars being formed; and (2) the state of the gas morphology and dynamics will shed light on why these galaxies will soon stop forming stars.

Section 2 describes the blue early-type sample. The pilot observations and data processing methods are described in Section 3. We discuss the radio continuum and H I imaging results in Sections 4 and 5, respectively. Section 6 provides a summary of our results. The AB magnitude system is used throughout this work.

2 BLUE EARLY-TYPE GALAXIES

We obtain the photometric and spectroscopic data from the Sloan Digital Sky Survey (SDSS) Data Release 7 (DR7; York et al. 2000; Abazajian et al. 2009) for all objects classified as 'galaxy' (Strauss et al. 2002). The sample of 204 low-redshift ($0.02 < z < 0.05$) blue ETGs were identified using the SDSS (Adelman-McCarthy et al. 2008) and the Galaxy Zoo project (Lintott et al. 2008, 2011; Schawinski et al. 2009b). The blue ETGs account for 5.7 per cent of all ETGs found within the same redshift range and are the most actively star-forming population of ETGs (Schawinski et al. 2009b). Further description of the blue ETG selection can be found in Schawinski et al. (2009b) and at http://data.galaxyzoo.org.

2.1 The pilot sample

To investigate the fate of the gas reservoir when star formation is quenched, we select four ETGs with comparable stellar masses and ultraviolet (UV)/optical colours indicative of rapid quenching: all four lie in the optical $u - r$ green valley, indicating they have significant intermediate-age stellar populations, and their near-ultraviolet (NUV) $- u$ UV/optical colours range from very blue, consistent with ongoing star formation (J1237+39), to the redder colours of passive, quenched galaxies (J0836+30) – see Fig. 1. Because of the diffused nature of H I gas, we have also selected the nearest galaxies which can be observed by the WSRT. The optical/stellar morphologies of this sample are presented in the top row of Fig. 2.

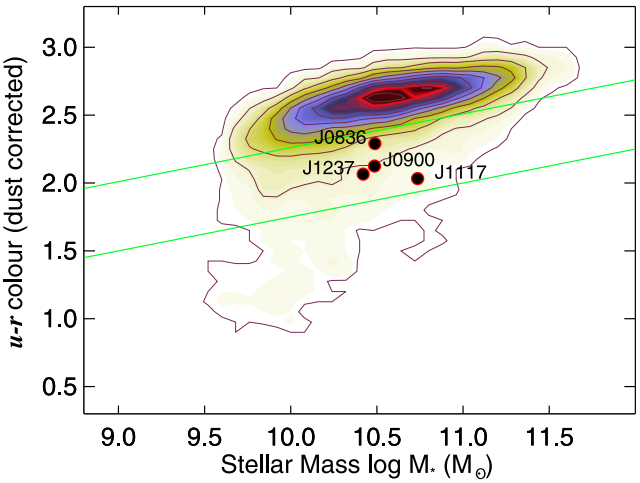

Figure 1. Colour–stellar mass diagram of ETGs found from SDSS and Galaxy Zoo. The contours represent the number density of ETGs occupying the colour–stellar mass region known as the 'red sequence'. All four pilot sample galaxies are located in the optical 'green valley' of the colour–mass diagram (as demarcated between the solid green lines). All galaxies show the presence of intermediate-age stellar populations by their 'green' $u - r$ colour.

Stellar population modelling find two distinct star formation truncation time-scales for early- and late-type galaxies whereby the ETGs appear to have fast quenching time-scales ($\leq$1 Gyr), while the late-type galaxies have quenching time-scales of several Gyr (Schawinski et al. 2014). Fig. 3 illustrates the different evolutionary stages represented by each of the four ETGs selected for this pilot study on a UV/optical colour–colour diagram. The colour of model stellar populations along different star formation quenching tracks is shown as solid lines where each large circle marks 1 Gyr and intervals of 100 Myr being shown by small circles along the stellar evolution tracks. The black shaded contours represent the low-redshift early-type population and the green contour represents the population of blue ETGs selected from Schawinski et al. (2009b). The observed stellar populations of J0836+30 and J0900+46 appear to be relatively evolved along the fastest quenching evolutionary pathway that occurs on time-scales of several hundred Myr to 1 Gyr (Schawinski et al. 2014). On the other hand, the stellar population colours of J1117+51 and J1237+39 are less evolved and consistent with earlier stages of quenching. We note that J1117+51 and J1237+39 appear to favour slower quenching pathways in Fig. 3. However, this could be due to differences between the start times for quenching in these galaxies relative to the fiducial starting point for quenching in the models. The H I properties of each sampled galaxy appear to be consistent with its respective evolutionary stage. See Section 5 for more details of the observed H I properties of this sample.

In addition, all four galaxies show optical emission lines dominated by activity other than star formation: J0836 and J0900 show Seyfert-like lines while J1117 and J1237 show low-ionization lines

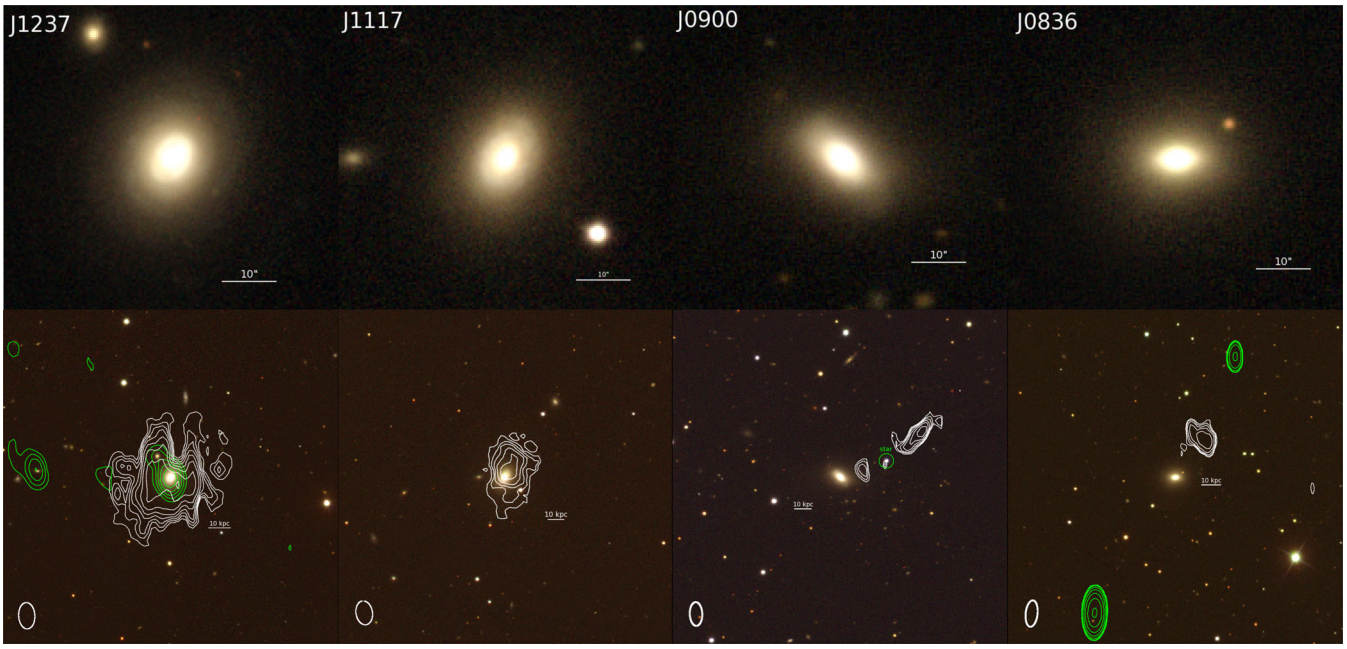

Figure 2. Top row: optical *gri* SDSS (Ahn et al. 2014) composite images of the four blue ETGs in our sample. The galaxies are arranged from left to right in terms of NUV − *u* colour from blue to red as a tracer of time. The white scale bars represent 10 arcsec. Bottom row: zoomed-out optical images with the WSRT radio observations overlaid. The white contours (asinh stretch) represent the H I and the green contours (logarithmic stretch) the unresolved radio continuum emission. The only resolved radio continuum emission is found for J1237 (the first panel from the left). The lowest radio and H I contours begin at 3σ and the highest contour is matched to the peak flux density of 0.87, 1.51, 0.86 and 44.79 mJy beam^{-1} for J1237, J1117, J0900 and J0836, respectively. It should be noted that the nuclear 1.4 GHz continuum unresolved point sources are not shown for J0900 and J1117 to avoid confusion with the H I contours.

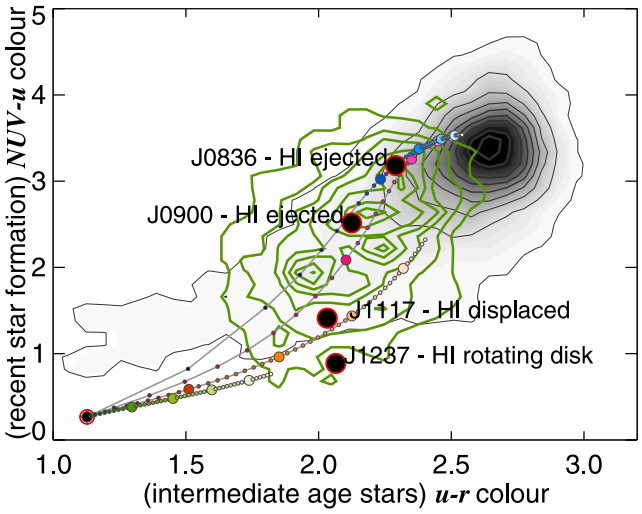

Figure 3. The UV/optical colour–colour diagrams of blue ETGs (thick green density contours) and the entire ETG population (thin black shaded contours). The model stellar population tracks with varying quenching timescales from Schawinski et al. (2014) are also overlaid. The large and small circles along the evolutionary tracks represent 1 Gyr and 100 Myr, respectively. Two out of four pilot sample galaxies show an absence of very young stellar populations indicated by NUV − *u* colours. Those three galaxies also show either a displaced H I reservoir (J1117+51) or a completely ejected H I reservoir (J0836 and J0900). The galaxy which is bluest in NUV − *u* features a rotating H I disc.

which could be due to black hole accretion, shocks or evolved stars (Sarzi et al. 2010). Fig. 4 presents the Baldwin–Phillips–Televich (BPT) diagnostic diagram (Baldwin, Phillips & Terlevich 1981) which shows the emission line ratios observed for blue ETGs. Table 1 lists the optical properties of this pilot sample. Stellar masses were obtained from spectral fitting (Schawinski et al. 2009b).

3 PILOT SURVEY

3.1 Radio observations

We performed imaging of the 1.4 GHz radio continuum and the atomic hydrogen (H I) emission of our pilot sample using the WSRT in the Netherlands between 2012 June and November. As the WSRT is an east–west interferometer, our observations were divided into several epochs to optimize the *uv* coverage. The single 20-MHz band is sampled over 1024 channels in the maxi-short baseline configuration in order to obtain a spectral resolution of 4 km s^{-1} spanning the range of 4000 km s^{-1}.

Using this set-up, a 24-h on-source integration should result in an rms noise level of 0.54 mJy beam^{-1} at full angular resolution over a full width at half-maximum (FWHM) of 8.25 km s^{-1} in velocity – corresponding to a column density sensitivity of 1.46×10^{19} atoms cm^{-2} per resolution assuming a uniform weighting.[1] Because of timetabling constraints, we were not able to obtain 24-h on-source integration for each of the four galaxies. Total integration times for each galaxy, the resultant synthesized beam properties and sensitivities are listed in Table 2.

3.2 Data processing

The observations are calibrated and processed in the standard manner using the MIRIAD reduction software (Sault, Teuben & Wright

[1] Noise estimations are obtained from the WSRT exposure time calculator found at http://www.astron.nl/oosterlo/expCalc.html

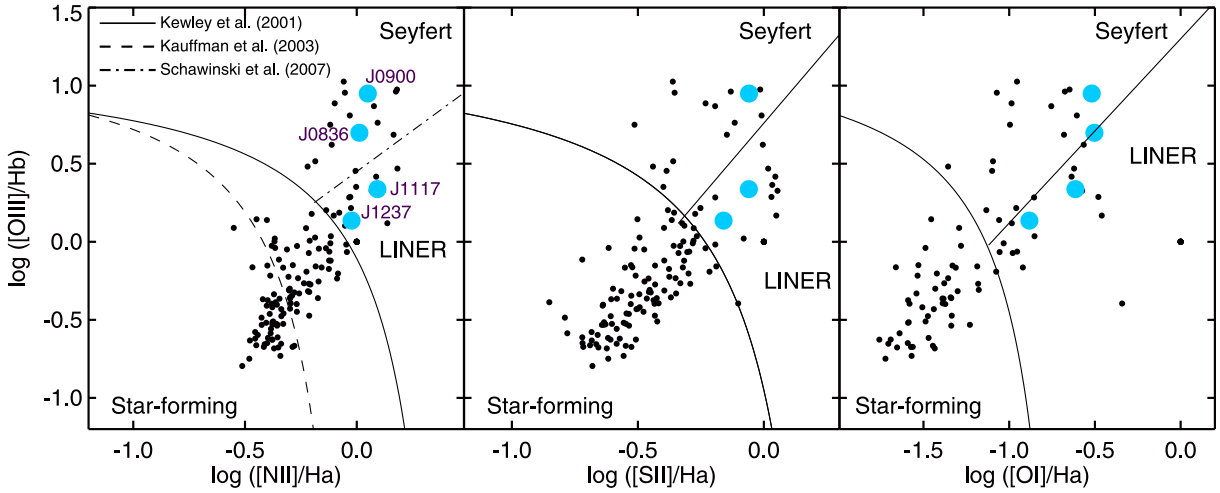

Figure 4. Optical nebular emission line diagrams. The nebular emission line ratios of the entire Schawinski et al. (2009b) sample of blue ETGs are plotted as small black points. The large blue solid points represent the objects selected in this pilot sample. The solid and dashed lines are two lines used to separate the nebular emission originating from star formation rather than that of nuclear Seyfert or LINER activity (Kewley et al. 2001; Kauffmann et al. 2003). The dotted–dashed line differentiates between ionization levels obtained from LINER versus Seyfert cores (Schawinski et al. 2007).

Table 1. Optical properties of our low-redshift blue ETG sample.

SDSS ID (1)	Galaxy (2)	RA (J2000) (3)	Dec. (J2000) (4)	Redshift (5)	Distance (6)	r (7)	$u-r$ (8)	$\log(M_\star)$ (9)
587735044686348347	J0836+30	08:36:01.5	+30:15:59.1	0.02561	105	−21.1	2.27	10.7
587731887888990283	J0900+46	09:00:36.1	+46:41:11.4	0.02748	113	−21.3	2.20	10.5
587732135382089788	J1117+51	11:17:33.3	+51:16:17.7	0.02767	115	−21.4	2.33	10.6
587738946685304841	J1237+39	12:37:15.7	+39:28:59.3	0.02035	84	−20.9	2.16	10.3

Notes. Column (1): SDSS object identification; column (2): galaxy identification used in this paper; column (3): galaxy centre's right ascension; column (4): galaxy centre's declination; column (5): redshift; column (6): distance in Mpc; column (7): SDSS r-band magnitude; column (8): optical $u-r$ colour; column (9): log (stellar mass) in solar mass as estimated by spectral fitting.

Table 2. WSRT observation summary. WSRT observation integration times and resulting beam properties are detailed for each of our pilot blue galaxies.

Galaxy (1)	Observations dates (2)	Total integration time (3)	Beam size (4)	Beam position angle (5)	$\mathrm{rms_{H\,I}}$ (6)	$\mathrm{rms_{1.4}}$ (7)
J0836+30	Nov 15, 25	20.3	29.5, 13.9	−2.0	4.1	0.083
J0900+46	Oct 23, Nov 11	10.3	24.0, 12.1	−1.7	11.0	0.062
J1117+51	June 30, Nov 18	24.0	19.8, 14.5	9.6	3.7	0.082
J1237+39	Aug 24, Oct 25, Nov 21	24.2	27.6, 17.5	4.7	32.6	0.038

Notes. Column (1): galaxy identification; column (2): observation dates; column (3): total on-source integration time in hours; column (4): synthesized beam diameter in arcseconds; column (5): synthesized beam position angle in degrees; column (6): rms noise level for the H I emission in mJy beam^{-1}; column (7): rms noise level for the 1.4 GHz radio continuum in mJy beam^{-1}.

1995). After the initial bandpass calibration using a WSRT standard calibrator, continuum images are produced and improved by iteratively applying a continuum self-calibration. The resulting calibration tables are then used for the line imaging as well. After a second continuum subtraction, the resulting H I image cubes are produced by using a robust weighting of 0.4 in order to produce the optimal balance between angular resolution and surface brightness sensitivity. We average across every second channel to improve the signal-to-noise sensitivity which results in a velocity resolution of 8.5 km s^{-1} (after Hanning smoothing). It should be noted that these final reduction parameters were determined after we had already tested various combinations of weighting schemes (including natural and uniform weightings) with different angular and frequency tapering for each set of observations. Table 2 lists the rms levels obtained for each galaxy in our sample.

4 RADIO CONTINUUM PROPERTIES OF BLUE EARLY-TYPE GALAXIES

We observe 1.4 GHz radio continuum emission in the nuclear regions of J0900+46, J1117+51 and J1237+39. No nuclear radio emission was found for J0836+30, but we do observe two radio lobes extending 88.4 kpc north-west and 102.5 kpc south-east of J0836+30 along the same direction as the extragalactic H I cloud.

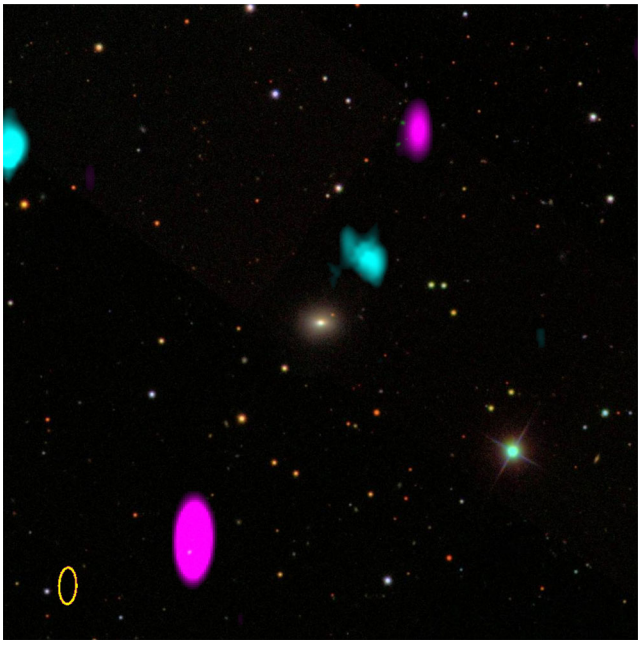

Figure 5. Multicolour composite of the J0836+30 field (centred on J0836+30) where the background colour image is a multicolour composite of the five SDSS optical *ugriz* bands. North and east are aligned to the top and left of the image. The H I reservoir (cyan) is observed to be offset to the north-east of the galaxy and lies linearly between the two 1.4 GHz unresolved radio continuum lobes (magenta). The yellow ring in the bottom-left of the figure represents the beam of these pilot radio observations.

Fig. 5 shows a multicolour composite image of the J0836+30 field where the radio continuum and the integrated H I emission are shown in magenta and cyan, while the background three-colour image is produced from the five SDSS *ugriz* bands. Further discussion of the possible mechanism for the displacement of the H I reservoir in J0836+30 can be found in Section 5.1.

We argue that the two radio lobes flanking both sides of J0836+30 are likely to be faded radio lobes belonging to J0836+30 and not likely to be due to a chance alignment with background sources. Although there is some overlap between the south-eastern radio lobe with a *Wide-field Infrared Survey Explorer* (*WISE*) 3.6-μm source, we do not find an optical/infrared (IR) counterpart for the north-western radio lobe. In addition, the projected separation between both lobes and J0836+30 is similar enough for the differences in angular separation (as well as brightness) to be accounted for by projection effects.

The nuclear radio luminosities range from 2.0×10^{35} to 7.4×10^{35} erg s^{-1} (or 1.0×10^{20} to 3.7×10^{21} W Hz^{-1}) and are consistent with those found mostly in other radio studies of low-redshift star-forming galaxies (Mauch & Sadler 2007; Jarvis et al. 2010). For J0836+30, the luminosities of the radio lobes in the north-west and south-east directions are 9.26×10^{35} and 1.22×10^{37} erg s^{-1}, respectively. Table 3 lists the measured 1.4 GHz radio continuum properties. Fig. 2 shows the radio continuum emission as green contours and the H I emission as white contours for the entire pilot sample.

Assuming that the nuclear radio continuum emission is due to star formation, we can estimate the star formation rate upper limits in our pilot sample. Using the star formation rate calibrations from Bell (2003) and Hopkins et al. (2003), we find that our galaxies have star formation rates that are fewer than 2 M$_\odot$ yr^{-1}. J1117+51 has the highest estimated star formation rate with 1.7 M$_\odot$ yr^{-1}.

Archival *IRAS* 60 μm observations (Moshir et al. 1990) were found for J1117+51 and J1237+39. Using the far-infrared to radio correlation (FRC) of low-redshift star-forming galaxies (Yun, Reddy & Condon 2001), we find that the expected far-IR 60 μm luminosity that correlates to our measured radio luminosity if the radio emission is due solely to star formation is log L_{60} of 9.6 and 9.0 for J1117+51 and J1237+39, respectively. In comparison to the *IRAS* log L_{60} values of 9.4 and 9.3, we find that the predicted values from the FRC are consistent with the idea that the 1.4 GHz continuum emission originates from star formation for both J1117+51 and J1237+39. It should be noted that the FRC has a scatter of approximately 0.25 dex and the *IRAS* measurement uncertainties are at the 20 per cent level.

Although the radio continuum emission observed from J1237+39 appears to be extended, it is in fact the result of a chance alignment between J1237+39 and a projected background galaxy, SDSS J123716.92+392921.9, which is 8.5 times more distant (at redshift $z = 0.176$) than J1237+39. Fig. 6 shows that the observed radio emission can be simply modelled by two point sources. The lack of any regions which display a flux excess or a flux deficit in our residual image (panel c of Fig. 6) is consistent with the idea that the radio emission from J1237+39 does not have an extended diffuse component.

5 H I CONTENT OF BLUE EARLY-TYPE GALAXIES

As the four blue ETGs in our sample represent four separate stages of evolution (as traced by the UV/optical colours and the [O III]/[Hβ]

Table 3. Radio (1.4 GHz) and H I properties of blue ETGs.

Galaxy (1)	$S_{1.4}$ (2)	$L_{1.4}$ (3)	$L_{1.4}$ (4)	SFR$_{1.4}$ (5)	$S_{\rm HI}$ (6)	$v_{\rm HI}$ (7)	$w_{\rm HI}$ (8)	$M_{\rm HI}$ (9)
J0836+30	$<2.5 \times 10^{-4}$	$<3.3 \times 10^{20}$ [a]	$<6.6 \times 10^{34}$	<0.4	0.078 (0.025)	7705	140	2.0 (0.7)
J0900+46	$9.7(2.4) \times 10^{-4}$	1.5×10^{21}	3.0×10^{35}	1.1	0.410 (0.182)	8277	62	12.3 (5.5)
J1117+51	$23.4(3.8) \times 10^{-4}$	3.7×10^{21}	7.4×10^{35}	1.7	0.100 (0.020)	8185	140	3.1 (0.6)
J1237+39	$12.0(1.6) \times 10^{-4}$	1.0×10^{21}	2.0×10^{35}	0.7	2.448 (0.403)	6096	245	40.8 (6.7)

Notes. Column (1): galaxy identification; column (2): total 1.4 GHz radio continuum emission in Jansky; column (3): radio continuum luminosity (1.4 GHz) in W Hz^{-1}; column (4): radio continuum luminosity (1.4 GHz) in erg s^{-1}; column (5): estimated star formation rate using the calibration by Bell (2003) and Hopkins et al. (2003) in M$_\odot$ yr^{-1}; column (6): integrated H I emission in Jansky; column (7): H I radial velocity as measured from the mid-point at FWHM in km s^{-1}; column (8): the 50 per cent H I velocity width in km s^{-1}; column (9): total H I mass in units of $\times 10^8$ M$_\odot$. Values in brackets give the estimated errors.
[a]Note that the luminosities of the radio lobes in the north-west and south-east directions are $4.63(\pm 0.44) \times 10^{21}$ and $6.12(\pm 0.03) \times 10^{22}$ W Hz^{-1}, respectively.

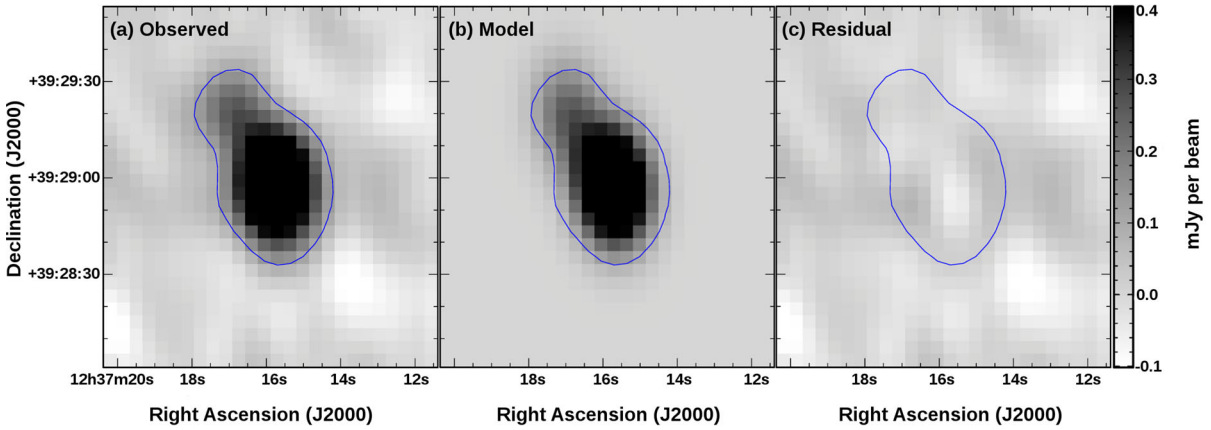

Figure 6. The 1.4 GHz radio continuum emission from J1237+39. Centred on J1237+39, we model the emission as two overlapping point sources. The solid blue line in all three panels marks the 3σ flux level of the observed 1.4 GHz emission (see panel a). Panels (b) and (c) show the model of two point sources and the residual maps, respectively.

ratios), we observe a correlation with their respective H I gas-to-stellar mass fractions whereby the gas fractions decrease as a function of time with increasing UV/optical colours and increasing [O III]/[Hβ] ratios. Table 3 lists the measured H I properties. The galaxy at the earliest stage of quenching in our sample (i.e. the galaxy with the bluest NUV/optical colour and the weakest [O III]/[Hβ] ratio), J1237+39, features a central, undisturbed, rotating H I disc. Both spatial and kinematic asymmetries are not observed in this galaxy (see Figs 2 and 7).

In the second bluest galaxy, J1117+51, the H I gas appears to be mostly within J1117+51. However, the gas morphology is fairly asymmetric and appears offset from the optical centre of the galaxy. Assuming the optical velocity to be the systemic velocity of each galaxy, we find the H I gas in J1117+51 to be largely blueshifted by up to 170 km s^{-1} from the galaxy's systemic velocity (see Fig. 7).

In the redder galaxies and the galaxies with stronger [O III]/[Hβ] ratios – indicative of ionization levels consistent with Seyfert activity – the H I reservoirs of J0836+30 and J0900+46 are completely displaced from their respective galaxy centres by 14–86 kpc. In addition, we find a significant amount of redshifted H I (by ≈70–80 km s^{-1}) with respect to the systemic velocity of the individual galaxy (see Fig. 2).

In J0836+30, the entire gas reservoir is offset spatially by 1 arcmin (projected distance of 30.5 kpc). To approximate the time-scale for the displacement of the gas reservoirs from J0836+30 and J0900+36, we simply divided the projected distances of the gas clouds by the observed H I velocity offsets from the systemic velocities taken from the optical observations. For J0836+30, the time-scale for the gas reservoir to have reached its current projected distance is approximately 373 Myr. Similarly, the H I emission detected near J0900+46 spans between 14 and 86 kpc from the optical centre of J0900+46 and appears to be redshifted by approximately 70 km s^{-1} (Fig. 8b). We estimate the displacement time-scale to range between 0.2 and 1.2 Gyr.

5.1 Mechanisms for the removal of H I

Support for the hypothesis that the observed H I clouds in the vicinity of J0836+30 and J0900+46 have been removed from their parent galaxy come from two main arguments. First, the proximity of the gas clouds is very similar to the distances between the Milky Way and its high velocity clouds (HVCs). Secondly, neither J0836+30 nor J0900+46 resides in dense environments with close neighbouring galaxies which could be responsible for stripping the gas reservoirs from each of these galaxies. In fact, Verley et al. (2007) have that found both J0836+30 and J0900+46 to be isolated galaxies using different galaxy isolation metrics. Several other previous studies have also classified J0836+30 to be a prototypical isolated galaxy (Karachentseva 1973; Stocke et al. 2004; Verdes-Montenegro et al. 2005).

In dense galaxy environments, such as clusters or compact galaxy groups, intergalactic gas clouds are not uncommon (Kilborn et al. 2000; Oosterloo & van Gorkom 2005; Borthakur, Yun & Verdes-Montenegro 2010) due to various gravitational and hydrodynamic interaction processes such as galaxy–galaxy interactions (Mihos 2004), harassment (Moore et al. 1996; Moore, Lake & Katz 1998), ram pressure and turbulent viscous stripping (Vollmer, Cayatte, Balkowski & Duschl 2001).

Ram pressure stripping is unable to shift such large amounts of gas using simple Toomre and Toomre pressure arguments (e.g. Chung et al. 2007). Also, the galaxies in this pilot sample do not have nearby galaxy neighbours nor do they reside in dense galaxy environment such as clusters or compact groups.

Nearby examples where the majority of the galaxy's gas is displaced via tidal stripping also result in strong morphological distortions (e.g. NGC 4438 in the Virgo Cluster; Hota, Saikia & Irwin 2007). Hota et al. (2012) have also identified a post-merger system, NGC 3801, where the extraplanar H I resulting from the merger has yet to be encountered by a newly triggered radio jet. As we do not observe any strong optical signatures from our galaxies such as stellar tidal tails, we can only infer that (1) the tidal features resulting from the strong interaction that removed the large gas mass have faded; or (2) another physical mechanism is responsible for the gas removal.

In the latter case, we posit that an active central engine has the required energy to expel a galaxy's gas. In the case of J0836+30, we observe two radio lobes in the same direction as the ejected H I cloud. This is suggestive that at earlier epochs, J0836+30 hosted a radio AGN which may have blown out the gas cloud that we observe. This hypothesis is consistent with recent studies which have found nuclear activity to be more prevalent in star-forming galaxies relative to weakly star-forming or quenched galaxies (Rosario et al. 2013).

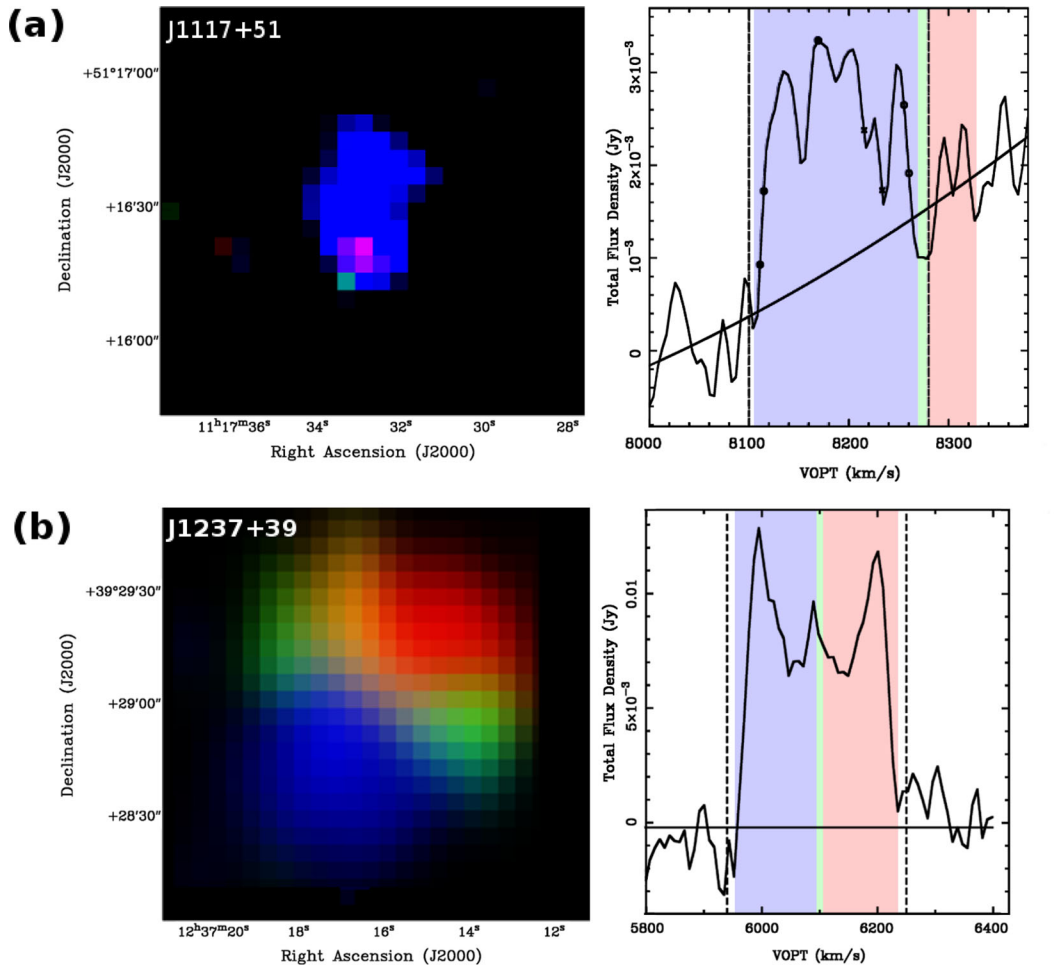

Figure 7. Velocity maps and spectra of J1117+51 (panel a) and J1237+39 (panel b). The three-colour velocity maps correspond to the H I emission in the velocity range highlighted in the same colour on the corresponding velocity spectrum. It should be noted that the green represents the optical velocity which we assume to be the systemic velocity of each of the blue early-types sampled in this paper. J1237+39 is the only galaxy in this sample for which rotation is observed in the H I (where the lower radial velocities are found on the south-east side of the gas reservoir).

As the displacement time-scale for this cloud is estimated to be ≈373 Myr, it is conceivable that J0836+30 has since evolved to a more Seyfert state (as observed via the optical nebular emission). A test of this hypothesis would be the presence of ionized gas adjacent to and between the observed H I cloud and the galaxy. Therefore, in the case of J0836+30, we think that the alignment between the radio lobes and the extragalactic H I cloud is more suggestive of gas ejection via radio jets than a previous tidal encounter whose tidal signatures have since faded in the past 373 Myr.

Previous observations of AGN-driven gas outflows have so far been from studies where the outflows are determined from the kinematic structures of the emitting or absorbing gas (Gopal-Krishna & Irwin 2000; Nesvadba et al. 2009; Mahony et al. 2013; Morganti et al. 2013). However, recent observations of ^{12}CO(1–0) emission from high-redshift radio galaxies have found spatial offsets between the molecular gas reservoir and their host galaxies on the scales of several tens of kiloparsec and aligned in the same direction to the radio hotspots/lobes (Emonts et al. 2014). We propose that we are witnessing a similar ejection of cold gas in J0836+30.

In the case of J0900+46, we observe neither strong radio continuum emission nor nearby galaxies which could remove the gas from this galaxy.

We posit that the observed extragalactic gas clouds in J0836+30 and J0900+46 are outflows and not inflows for two reasons. First, if the observed cold clouds were being accreted, the source of this gas is either a neighbouring galaxy or primordial gas leftover from galaxy formation. However, neither galaxies have neighbouring galaxies and the accretion of primordial gas at the current epoch is in a warm-hot phase rather than that of the observed cold H I. Secondly, Bouché et al. (2012) found that gas outflows are usually found at angles nearly orthogonal (>60°) to the plane of the galaxy, whereas inflows have small azimuthal angles (<30°) to the galactic plane. Therefore, we think that it is more likely that our observed extragalactic H I clouds originated from our target galaxies.

The mass of our gas clumps is approximately the total mass of HVCs around the Milky Way, the Large Magellanic Cloud (LMC) and the Small Magellanic Cloud (SMC). Assuming that our observed gas clumps are analogous to these HVCs, we can expect a similar gas dissipation time on the order of several hundred million years if there is not some sort of support mechanism that prevents or slow down against cloud dissipation (Putman, Peek & Joung 2012). The cloud survival time is linked closely to its total mass, cloud density, relative halo density and velocity (Putman et al. 2012). Previous studies have found that while the least bound material is

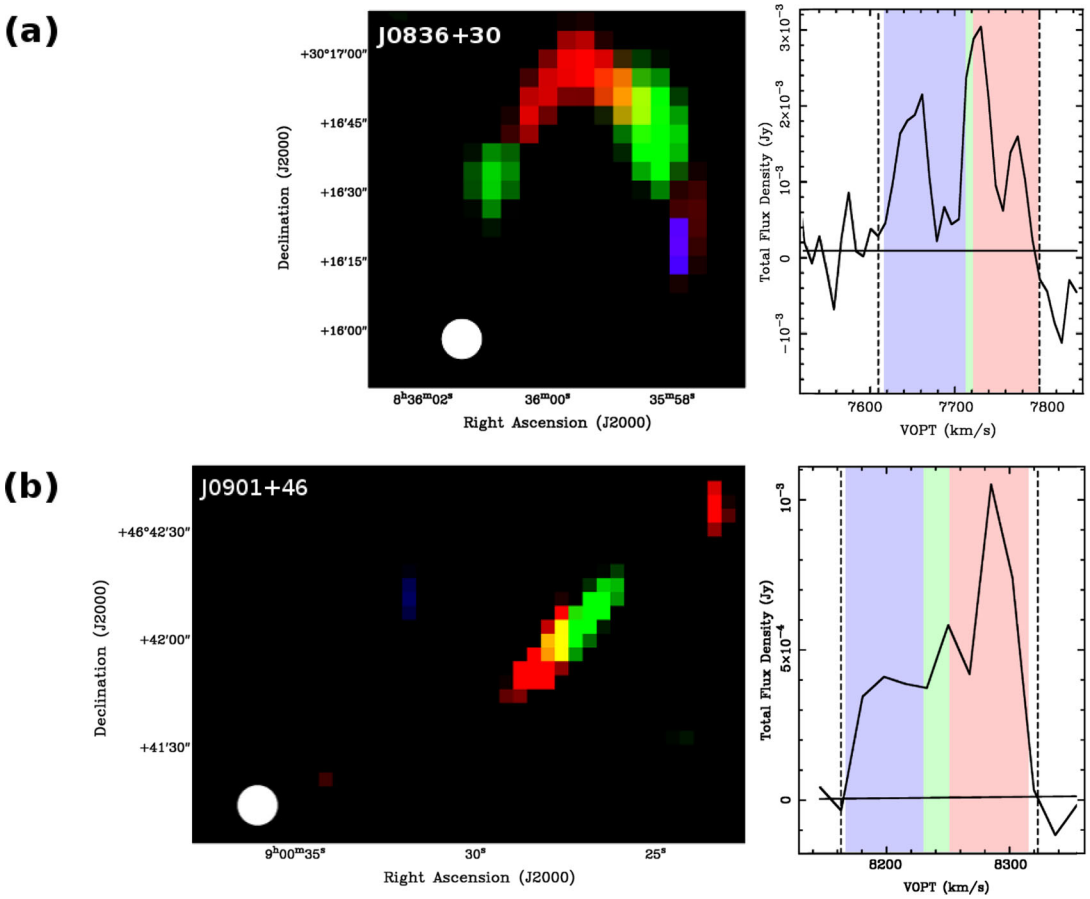

Figure 8. Velocity maps and spectra of J0836+30 (panel a) and J0900+46 (panel b). The three-colour velocity maps correspond to the H I emission in the velocity range highlighted in the same colour on the corresponding velocity spectrum. The white solid circle represents the position of the blue ETG relative to the observed H I emission. It should be noted that the green represents the optical velocity which we assume to be the systemic velocity of each of the blue early-types sampled in this paper.

likely to expand out into the intergalactic medium (IGM), bound structures are likely to fall back on to the galaxies in less than 1 Gyr (Hibbard & Mihos 1995; Hibbard & van Gorkom 1996).

5.2 H I gas fractions

Using the scaling relations from the α40 catalogue of the Arecibo Legacy Fast ALFA (ALFALFA) survey (Huang et al. 2012), star-forming galaxies with the stellar masses of J0836+30 and J0900+46 would be expected to have average H I masses of approximately 1×10^{10} and 8.7×10^{9} $M_{\odot}$, yet we observe only 2×10^{8} and 1.2×10^{9} $M_{\odot}$, respectively. This implies that some fraction of the gas may have been ionized and heated and we are currently only observing the remaining fraction of H I. The external H I clouds we observe represent the remnants of the original gas reservoirs swept out of the host galaxy, and from the present data it is not clear whether the missing H I was also expelled or heated or simply dissipated. Regardless, the displaced gas reservoir is required to complete the quenching of these galaxies and prevent further star formation.

Extrapolating from the Kennicutt–Schmidt star formation law, the correlation between the H I gas fraction and the star formation history traced by the NUV $-$ r colour provides a rough indicator for the cold gas surface density (Huang et al. 2012; Zwaan et al. 2013). Relative to gas-rich star-forming galaxies (mostly spirals; ALFALFA; Huang et al. 2012), low-redshift transition galaxies with stellar masses greater than 10^{10} $M_{\odot}$ (GALEX Arecibo SDSS Survey, GASS; Catinella et al. 2012) and nearby ETGs from the Atlas^{3D} survey (Serra et al. 2012; Cappellari et al. 2013; Young et al. 2014), we find that J1117−51 and J1237+36 have similar gas fractions and NUV $-$ r colours to E+A galaxies and straddle the region between star-forming galaxies with low gas fractions and that of gas-rich ETGs.

Fig. 9 compares the H I–stellar mass ratio and the integrated NUV $-$ r colour of J1117+51 and J1237+39 (marked as black stars) to those of E+A galaxies (represented by black crosses) where H I has been previously detected (Chang et al. 2001; Buyle et al. 2006; Helmboldt 2007; Zwaan et al. 2013). Galaxies from ALFALFA are represented by blue solid points and the solid line marks the average colours and average gas fractions found from GASS. NUV measurements of our sample were obtained from the *Galaxy Evolution Explorer* (*GALEX*) satellite telescope via the NASA Extragalactic Database.[2]

We also compare our pilot sample of blue ETGs to recent H I observations of nearby ETGs from the Atlas^{3D} survey (Serra et al. 2012). The Atlas^{3D} ETGs with regularly rotating undisturbed H I morphologies are represented by open circles, while, Atlas^{3D} galaxies with very disturbed and unsettled H I morphologies and

[2] http://ned.ipac.caltech.edu

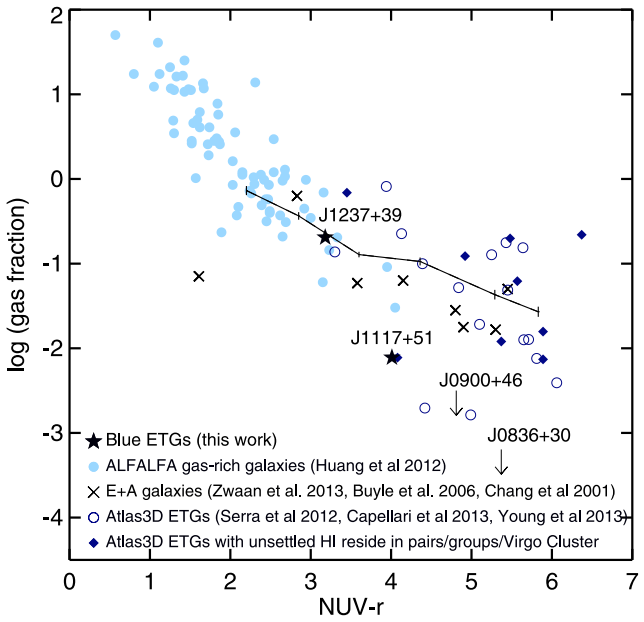

Figure 9. H I-to-stellar mass ratio as a function of galaxy colour. The solid line shows the average gas fractions found from GASS survey of massive transition-type galaxies (Catinella et al. 2012).

kinematics are represented by solid diamonds in Fig. 9. It should be noted that all the Atlas^{3D} ETGs with disturbed H I morphologies reside in group or Virgo Cluster environments. Also, for a given NUV $-$ r colour, these Atlas^{3D} galaxies have higher gas fractions than that of the E+A or blue ETG samples. This suggests that either (1) the Atlas^{3D} ETGs where H I is observed are at earlier stages of evolution than the sample of E+A galaxies or blue ETGs; or that (2) the merger scenario is as likely to result in an increase in gas fraction as it is to a reduction. Upper limits are shown for J0836+30 and J0900+46 due to the lack of H I within the host galaxies.

We find the H I gas fraction and NUV $-$ r colour of J1237+39 (the galaxy at the earliest stage of quenching) to be very comparable to those of star-forming galaxies from both the ALFALFA and GASS surveys. On the other hand, the gas fractions for the three more evolved blue ETGs in our sample are significantly lower than the average gas fractions expected from star-forming galaxies, transitioning galaxies or even gas-rich ETGs with similar NUV $-$ r colours. Similar to our results, the gas fractions of post-starburst E+A galaxies are lower than the average gas fractions for any given NUV $-$ r colours. The combination of the H I mapping and the radio continuum observations of J0836+30 and J0900+46 suggests that the star formation in these two galaxies will be truncated soon. This result is consistent with those of Schawinski et al. (2009a) who were unable to detect any significant molecular gas reservoirs within Green Valley galaxies with Seyfert ionization properties.

As previously seen in Fig. 3, these pilot H I observations show that the main mechanism for the fast quenching of star formation in blue early-types is due to the physical displacement of the main gas reservoir from which stars are formed. Hence, it is likely that the depressed gas fractions from our sample (see Fig. 9) are due to a fast quenching process (relative to other evolving galaxies) which removes a significant fraction, if not the entire gas reservoir, from which stars are formed.

Should the gas fall back, it may restart minor star formation which may be visible as the frosting $\approx$1 per cent mass fraction of young stars often observed in quenched ETGs (Yi et al. 2005; Schawinski et al. 2006; Kaviraj et al. 2007). While it may cause frosting, this returning gas however will not return the host galaxy to self-regulated star formation on the main sequence. An alternative fate for the ejected gas is that it persists at large distances from the quenched galaxy, as is observed in the Milky Way (in the form of the starless Magellanic Stream; For et al. 2014); as well as in many quenched ETGs (e.g. Serra et al. 2012).

5.3 Argument against coincident dark galaxies

Dark galaxies can be typically defined as the extreme end of low surface brightness galaxies where few stars are found, consisting mainly of gas. With respect to our observed extraplanar gas clumps, it is very unlikely that these gas clumps are neighbouring dark galaxies. Current reionization models of the Universe predict the latter as they find that the gas from 95 per cent of the low-mass systems ($M_{\rm virial} \leq 10^8$ M$_\odot$ or $v_{\rm circ} \leq 20$ km s^{-1}) appears to have been photoevaporated during the epoch of reionization (Susa & Umemura 2004).

Apart from a few reported cases of extragalactic gas clouds in group/cluster environments (Minchin et al. 2005; Davies et al. 2006) with no known optical counterparts, current and previous H I all-sky surveys such as ALFALFA (Haynes et al. 2011) and H I Parkes All-Sky Survey (HIPASS; Doyle et al. 2005; Wong et al. 2009) have not found any isolated extragalactic H I clouds devoid of stars. This is consistent with simple gas equilibrium models (Taylor & Webster 2005) which concluded that in the absence of an internal radiation field, dark galaxies/gas clouds with masses greater than 10^9 M$_\odot$ will become Toomre unstable against star formation and start forming stars. Galaxy evolution simulations demonstrated that the majority of gas clouds identified with no known optical counterpart can be easily reproduced by galaxy–galaxy interactions (Bekki, Koribalski & Kilborn 2005; Duc & Bournaud 2008).

6 SUMMARY

We have performed deep imaging of the H I content and 1.4 GHz radio continuum emission of four blue ETGs that are at four different stages of star formation truncation using the WSRT. The H I morphologies, kinematics and relative H I gas fractions are excellent probes and measures of the quenching evolutionary stages for each of our sample galaxy. A summary of our results are as follows.

(i) We observe nuclear 1.4 GHz radio continuum emission that is consistent with emission from star formation from three galaxies at the three earliest stages of quenching evolution, namely, J1237+39, J1117+51 and J0900+46 (in the order of earliest to later stages of evolution).

(ii) The galaxy at the earliest stage of quenching, J1237+39, also has the bluest NUV $-$ r colour, weakest [O III]/Hβ] ratio, the highest H I gas fraction and a symmetric rotating H I disc.

(iii) At more advanced stages of quenching evolution, we observe increasingly asymmetric and increased spatial offsets between the H I gas and the stellar component of the galaxy. Non-rotating H I gas kinematics are also observed. In the case of the two galaxies at the most advanced stages of evolution where Seyfert ionization signatures have been observed (J0900+46 and J0836+30), the H I gas reservoirs have been entirely expelled by approximately 14–86 kpc from their respective host galaxies. Because of the lack of neighbouring galaxies, it is difficult to attribute the stripped gas to tidal or ram pressure interactions.

(iv) In the galaxy at the most advanced quenching stage, J0836+30, the expelled gas reservoir is observed to be in alignment between the host galaxy and two radio lobes – suggesting the gas reservoir may have been swept out of the galaxy by powerful outflows from the central AGN in a previous active phase. This scenario is consistent with recent observations of AGN-driven gas outflows both locally and at higher redshifts (Sturm et al. 2011; Mahony et al. 2013; Morganti et al. 2013; Emonts et al. 2014).

(v) We conclude that the rapid quenching of star formation in low-redshift ETGs is due to the physical expulsion of the entire gas reservoir, rather than the exhaustion of gas via star formation. An AGN outflow has the necessary energy to expel the reservoir of cold gas. In addition, we do not think that AGN heating of the gas is a dominant mechanism because the H I gas would not remain visible as a coherent structure if this was the case.

ACKNOWLEDGEMENTS

We thank the anonymous referee for support of this project and for improving the manuscript. OIW acknowledges a Super Science Fellowship from the Australian Research Council and the Helena Kluyver visitor programme at ASTRON/JIVE. KS is supported by SNF Grant PP00P2 138979/1. The Westerbork Synthesis Radio Telescope is operated by the Netherlands Institute for Radio Astronomy (ASTRON) with support from the Netherlands Foundation for Scientific Research (NWO). This publication makes use of SDSS DR10 data. This research has made use of the NASA/IPAC Extragalactic Database (NED) which is operated by the Jet Propulsion Laboratory, California Institute of Technology, under contract with the National Aeronautics and Space Administration.

REFERENCES

Abazajian K. N. et al., 2009, ApJS, 182, 543
Adelman-McCarthy J. K. et al., 2008, ApJS, 175, 297
Ahn C. P. et al., 2014, ApJS, 211, 17
Alatalo K. et al., 2011, ApJ, 735, 88
Baldwin J. A., Phillips M. M., Terlevich R., 1981, PASP, 93, 5
Bekki K., Koribalski B. S., Kilborn V. A., 2005, MNRAS, 363, L21
Bell E. F., 2003, ApJ, 586, 794
Borthakur S., Yun M. S., Verdes-Montenegro L., 2010, ApJ, 710, 385
Bouché N. et al., 2010, ApJ, 718, 1001
Bouché N., Hohensee W., Vargas R., Kacprzak G. G., Martin C. L., Cooke J., Churchill C. W., 2012, MNRAS, 426, 801
Buyle P., Michielsen D., De Rijcke S., Pisano D. J., Dejonghe H., Freeman K., 2006, ApJ, 649, 163
Cappellari M. et al., 2013, MNRAS, 432, 1862
Catinella B. et al., 2012, A&A, 544, A65
Chang T.-C., van Gorkom J. H., Zabludoff A. I., Zaritsky D., Mihos J. C., 2001, AJ, 121, 1965
Chung A., van Gorkom J. H., Kenney J. D. P., Vollmer B., 2007, ApJ, 659, L115
Croston J. H., Hardcastle M. J., Kharb P., Kraft R. P., Hota A., 2008, ApJ, 688, 190
Croton D. J. et al., 2006, MNRAS, 365, 11
Davies J. I., Disney M. J., Minchin R. F., Auld R., Smith R., 2006, MNRAS, 368, 1479
Doyle M. T. et al., 2005, MNRAS, 361, 34
Duc P.-A., Bournaud F., 2008, ApJ, 673, 787
Elbaz D. et al., 2011, A&A, 533, A119
Emonts B. H. C., Morganti R., Tadhunter C. N., Holt J., Oosterloo T. A., van der Hulst J. M., Wills K. A., 2006, A&A, 454, 125
Emonts B. H. C. et al., 2014, MNRAS, 438, 2898
For B.-Q., Staveley-Smith L., Matthews D., McClure-Griffiths N. M., 2014, ApJ, 792, 43
Gopal-Krishna Irwin J. A., 2000, A&A, 361, 888
Harrison C. M., Thomson A. P., Alexander D. M., Bauer F. E., Edge A. C., Hogan M. T., Mullaney J. R., Swinbank A. M., 2014, (arXiv:e-prints)
Haynes M. P. et al., 2011, AJ, 142, 170
Heckman T. M., Best P. N., 2014, ARA&A, 52, 589
Helmboldt J. F., 2007, MNRAS, 379, 1227
Hibbard J. E., Mihos J. C., 1995, AJ, 110, 140
Hibbard J. E., van Gorkom J. H., 1996, AJ, 111, 655
Hopkins A. M., Afonso J., Chan B., Cram L. E., Georgakakis A., Mobasher B., 2003, AJ, 125, 465
Hota A., Saikia D. J., Irwin J. A., 2007, MNRAS, 380, 1009
Hota A. et al., 2011, MNRAS, 417, L36
Hota A., Rey S.-C., Kang Y., Kim S., Matsushita S., Chung J., 2012, MNRAS, 422, L38
Huang S., Haynes M. P., Giovanelli R., Brinchmann J., 2012, ApJ, 756, 113
Jarvis M. J. et al., 2010, MNRAS, 409, 92
Karachentseva V. E., 1973, Astrofizicheskie Issledovaniia Izvestiya Spetsial'noj Astrofizicheskoj Observatorii, 8, 3
Kauffmann G. et al., 2003, MNRAS, 346, 1055
Kaviraj S. et al., 2007, ApJS, 173, 619
Kaviraj S., Schawinski K., Silk J., Shabala S. S., 2011, MNRAS, 415, 3798
Kewley L. J., Dopita M. A., Sutherland R. S., Heisler C. A., Trevena J., 2001, ApJ, 556, 121
Kharb P., O'Dea C. P., Baum S. A., Colbert E. J. M., Xu C., 2006, ApJ, 652, 177
Kilborn V. A. et al., 2000, AJ, 120, 1342
Kormendy J., Ho L. C., 2013, ARA&A, 51, 511
Lilly S. J., Carollo C. M., Pipino A., Renzini A., Peng Y., 2013, ApJ, 772, 119
Lintott C. J. et al., 2008, MNRAS, 389, 1179
Lintott C. et al., 2011, MNRAS, 410, 166
Mahony E. K., Morganti R., Emonts B. H. C., Oosterloo T. A., Tadhunter C., 2013, MNRAS, 435, L58
Mauch T., Sadler E. M., 2007, MNRAS, 375, 931
Mihos J. C., 2004, in Mulchaey J. S., Dressler A., Oemler A., eds, Clusters of Galaxies: Probes of Cosmological Structure and Galaxy Evolution. Cambridge Univ. Press, Cambridge, p. 277
Minchin R. et al., 2005, ApJ, 622, L21
Moore B., Katz N., Lake G., Dressler A., Oemler A., 1996, Nature, 379, 613
Moore B., Lake G., Katz N., 1998, ApJ, 495, 139
Morganti R., Fogasy J., Paragi Z., Oosterloo T., Orienti M., 2013, Science, 341, 1082
Moshir M. et al., 1990, IRAS Faint Source Catalogue, version 2.0
Nesvadba N. P. H. et al., 2009, MNRAS, 395, L16
Noeske K. G. et al., 2007, ApJ, 660, L47
Nyland K. et al., 2013, ApJ, 779, 173
Oosterloo T., van Gorkom J., 2005, A&A, 437, L19
Peng Y.-J. et al., 2010, ApJ, 721, 193
Putman M. E., Peek J. E. G., Joung M. R., 2012, ARA&A, 50, 491
Rosario D. J. et al., 2013, ApJ, 771, 63
Sanders D. B., Soifer B. T., Elias J. H., Madore B. F., Matthews K., Neugebauer G., Scoville N. Z., 1988, ApJ, 325, 74
Sarzi M. et al., 2010, MNRAS, 402, 2187
Sault R. J., Teuben P. J., Wright M. C. H., 1995, in Shaw R. A., Payne H. E., Hayes J. J. E., eds, ASP Conf. Ser. Vol. 77, Astronomical Data Analysis Software and Systems IV. Astron. Soc. Pac., San Francisco, p. 433
Schawinski K. et al., 2006, Nature, 442, 888
Schawinski K., Thomas D., Sarzi M., Maraston C., Kaviraj S., Joo S.-J., Yi S. K., Silk J., 2007, MNRAS, 382, 1415
Schawinski K. et al., 2009a, ApJ, 690, 1672
Schawinski K. et al., 2009b, MNRAS, 396, 818
Schawinski K. et al., 2014, MNRAS, 440, 889
Serra P. et al., 2012, MNRAS, 422, 1835
Stocke J. T., Keeney B. A., Lewis A. D., Epps H. W., Schild R. E., 2004, AJ, 127, 1336

Strauss M. A. et al., 2002, AJ, 124, 1810
Sturm E. et al., 2011, ApJ, 733, L16
Susa H., Umemura M., 2004, ApJ, 610, L5
Taylor E. N., Webster R. L., 2005, ApJ, 634, 1067
Tojeiro R. et al., 2013, MNRAS, 432, 359
Verdes-Montenegro L., Sulentic J., Lisenfeld U., Leon S., Espada D., Garcia E., Sabater J., Verley S., 2005, A&A, 436, 443
Verley S. et al., 2007, A&A, 472, 121
Vollmer B., Cayatte V., Balkowski C., Duschl W. J., 2001, ApJ, 561, 708
Wong O. I., Webster R. L., Kilborn V. A., Waugh M., Staveley-Smith L., 2009, MNRAS, 399, 2264
Wong O. I. et al., 2012, MNRAS, 420, 1684
Yi S. K. et al., 2005, ApJ, 619, L111
York D. G. et al., 2000, AJ, 120, 1579
Young L. M. et al., 2014, MNRAS, 444, 3408
Yun M. S., Reddy N. A., Condon J. J., 2001, ApJ, 554, 803
Zwaan M. A., Kuntschner H., Pracy M. B., Couch W. J., 2013, MNRAS, 432, 492

This paper has been typeset from a TEX/LATEX file prepared by the author.